Iterative migration using sparseness constraints with the hyperbolic penalty function: Application on two 2-D field datasets

Mandy Wong and Antoine Guitton

ABSTRACT

Sparse reflectivities are obtained with iterative migration thanks to the hyperbolic penalty function for both data fitting and model styling goals. Sparseness is achieved by letting parts of the model treated in a "ℓ^1-norm" sense. Comparing with a more classical least-squares approach without regularization, the sparse-reflectivity images have less artifacts and better defined reflectors. However, these reflectors are often less continuous and the parameterization of the hyperbolic penalty function remains cumbersome. The main advantages of the hyperbolic penalty function, as opposed to other "ℓ^1-type" norms, is that it is convex, can behave like the ℓ^1 or ℓ^2 norms as needed, and can be minimized very efficiently with a fast non-linear conjugate direction method.

INTRODUCTION

This manuscript presents the follow up of our previous work (Wong and Guitton, 2014) on applying the hyperbolic penalty function to the iterative migration problem. Iterative migration poses the imaging problem as an inversion problem. Instead of applying the migration operator, which is regarded as the adjoint to the forward modeling operator, iterative migration aims to apply the inverse of the forward modeling operator to recover the reflectivity series of the subsurface. Due to the size of the problem, iterative migration is usually performed iteratively using gradient based techniques. Many studies have shown that the least-squares iterative migration image has fewer migration artifacts, better relative amplitude information, and higher resolution than the corresponding migration image (Clapp, 2005; Valenciano, 2008; Wong et al., 2012). In Wong and Guitton (2014) and for iterative migration, we used the hyperbolic penalty function (HPF) in the regularization term to recover a sharp and sparse reflectivity model in a 1D synthetic example. In addition, we have shown that when data are contaminated with non-Gaussian noise (e.g, noise bursts, spikes), the HPF for the data-fitting part is more robust in recovering the reflectivity series. The HPF with the correct parameterization for measuring data and model misfits is often a better choice than the standard ℓ^2 norm because it varies smoothly between the ℓ^2 norm for small residuals and ℓ^1 norm for high residuals. Therefore, the HPF can be made robust to outliers present in the data and can help build sparse models.

Being convex, a fast solver based on a non-linear conjugate direction method can be used to minimize the HPF efficiently (Claerbout, 2014).

We apply iterative imaging on two 2D field data examples using a HPF solver to get sparse reflectivity series and a ℓ^2 solver for our more traditional least-squares migration results. Note that both solvers use the previous search direction and the current gradient to find the optimal search path (Claerbout, 2014). The first dataset covers the region of a layered earth. The second dataset is located in a region with a salt structure. Inversion results with both datasets show that the iterative migration results with the HPF in the regularization term are sparse, with less migration artifacts and better signal content than their least-squares migration counterparts. These results rely heavily on our ability to select a judicious set of parameters controlling the ℓ^2/ℓ^1 behavior of the HPF, as well as the strength of the regularization term.

In this paper, we begin by introducing the HPF and the objective function we are minimizing. Next, we discuss the objective functions used in this study. Then we show with 2D field data examples how the iterative migration performs with the ℓ^2 and HPF solvers.

THEORY

We now present the hyperbolic penalty function and its main properties, as well as the objective functions used in this study.

Hyperbolic Penalty Function

The HPF (Claerbout, 2014) is a convex penalty function that varies smoothly from ℓ^2 to ℓ^1. Equation (1) below presents the HPF, $H(r)$, and its derivatives:

$$\begin{aligned} H(r) &= \sqrt{1+(\tfrac{r}{g})^2} - 1, \\ H'(r) &= \tfrac{r}{g\sqrt{1+(\frac{r}{g})^2}}, \end{aligned} \tag{1}$$

where g is a constant that scales the residual r. The first derivative, $H'(r)$, behaves like the first derivative of the ℓ^2 norm at small $|\frac{r}{g}|$. At large $|\frac{r}{g}|$, it behaves as the first derivative of the ℓ^1 norm. In practice, the factor g is often taken to be the value of some percentile of residual magnitudes. Its value determines what part of the residual is treated as ℓ^1 and what part is treated as ℓ^2. The HPF is minimized with a non-linear conjugate direction solver and is described in details in Claerbout (2014), Chapter 6.

Objective Function

In iterative migration, we expect the reflectivity model to be made up of a series of sharp and sparse signals. The basic objective function using the ℓ^2 norm is:

$$S_2(\mathbf{m}) = \|\mathbf{W}\,(\mathbf{Lm}-\mathbf{d})\,\|_2^2, \tag{2}$$

where $\mathbf{L}$ represents the Born modeling operator acting onto the reflectivity model $\mathbf{m}$, and $\mathbf{d}$ is the observed data. $\mathbf{W}$ is a data weighting function.

To promote the sparseness in the reflectivity model $\mathbf{m}$, we include a model-styling goal using the hyperbolic penalty function as measure of fitness. The desired objective function $S_{HPF}(\mathbf{m})$ becomes:

$$S_{HPF}(\mathbf{m}) = H_d(\mathbf{W}\,(\mathbf{Lm}-\mathbf{d})) + \epsilon H_m(\mathbf{m}), \tag{3}$$

where H_d and H_m are HPFs for the data-fitting and model-styling goals, respectively. Three constants need to be chosen in equation (3): two thresholds values g_d and g_m that regulate the transitioning behavior between ℓ^2 and ℓ^1 in the HPF, and ϵ that tunes the relative strength of the regularization with respect to the data-fitting goal.

After inspecting the two datasets, we concluded that no large spikes or bursts are present in the data. Therefore, we selected a large value for g_d such that the data-fitting function in equation 3 is effectively measured by the ℓ^2 norm. For simplicity, we will refer the inversion using equation 3 as the HPF iterative migration.

FIELD DATA EXAMPLES

The two 2-D datasets selected in this study were extracted from a 3-D survey carried out in the Gulf of Mexico. The maximum offset is about 4 km with a shallow water bottom at 500 m. This region has significant anisotropy (Li et al., 2014). Since we are using isotropic modeling, and considering that other physical processes are ignored (e.g., attenuation), we don't expect to fit all the information contained in the data.

We corrected for the 3D spherical spreading effects so that the data can better match the amplitude of the 2D modeling and migration operators. We apply the iterative migration in two regions: a sedimentary environment, and a region with a salt body. The inversion of these traces with and without HPF regularization, are presented here.

Sediment velocity model

Figure 1a shows a shot gather from the ExxonMobil data in the sediment area. This area contains mostly horizontally stratified layers with strong amplitudes recorded

from shallower reflections. As a result, we apply a diagonal data weighting (Figure 1b) in the iterative migration to emphasize the reflection energy from the deeper part of the model. Also, the data weighting excludes the direct arrival and head waves.

Figure 2a shows the migration velocity model. The velocity values increase from 1500 m/s to 4000 m/s in depth. There is a fault cutting diagonally across the model starting from a depth of 2000 m. Figure 2b shows the reverse-time migration (RTM) image. Figure 3a shows the inverted image using least-squares reverse time migration (LSRTM) after 12 iterations of conjugate gradient algorithm. Equation 2 shows the objective function for LSRTM. When compared to the RTM image, we clearly see the increased bandwidth of the inverted image (deconvolution effect). Some of the weaker reflectors become more apparent over iterations as shown in the annotation. However, the inversion tends to boost migration artifacts as well, thus increasing the overall noise level in the image.

Figure 3b shows the inverted image at iteration 20 using the hyperbolic penalty function (Equation 3) for $\epsilon = 0.00125$ and $g_m = 12.5$. The model-styling term in the objective function has enforced sparsity in the reflectivity solution. The addition of the sparseness constraints helps attenuate the artifacts in the shallow region that we could see in the least-squares migration result. However, the sparseness constraint tends to make some reflectors less continuous.

Figure 4a shows one shot gather from the input data. After 1 iteration, the data residual from LSRTM (Figure 4b) and HPF iterative migration (Figure 4b) drops significantly. At iteration 12, the least-squares migration data residual (Figure 4c) drops slightly with the stronger reflection energy being less coherent. Figure 4f shows the data residual from HPF iterative migration at iteration 20. Due to the presence of the model styling goal, the data fitting is a little bit less than the one in Figure 4c.

Figure 6 shows the normalized power spectra in the z-direction for the RTM, LSRTM, and HPF iterative migration images. Since the amplitude scale between migration and inversion images are different. We normalized the amplitude of the power spectra by scaling the maximum value to 1. We then converted the normalized amplitude into decibels. Notice that, with iterative inversion, the LSRTM and HPF spectrum becomes more white, especially in the higher and lower frequency range. The LSRTM spectrum shows a higher frequency content than the HPF one probably due to the increased noise content. In the HPF inversion, the high frequency noise is suppressed. The relative amplitude in the range of $kz = 0.004 - 0.012$ is higher than that from LSRTM.

Choosing epsilon and threshold values

Figure 5 shows 9 inverted images from the HPF iterative migration using different ϵ and g_m values for the sediment case. As expected, by increasing g_m for a constant ϵ the images become less sparse because more parts of the images are treated in a "ℓ^2 norm" sense and less in a "ℓ^1 norm" sense. Similarly, increasing ϵ for a constant

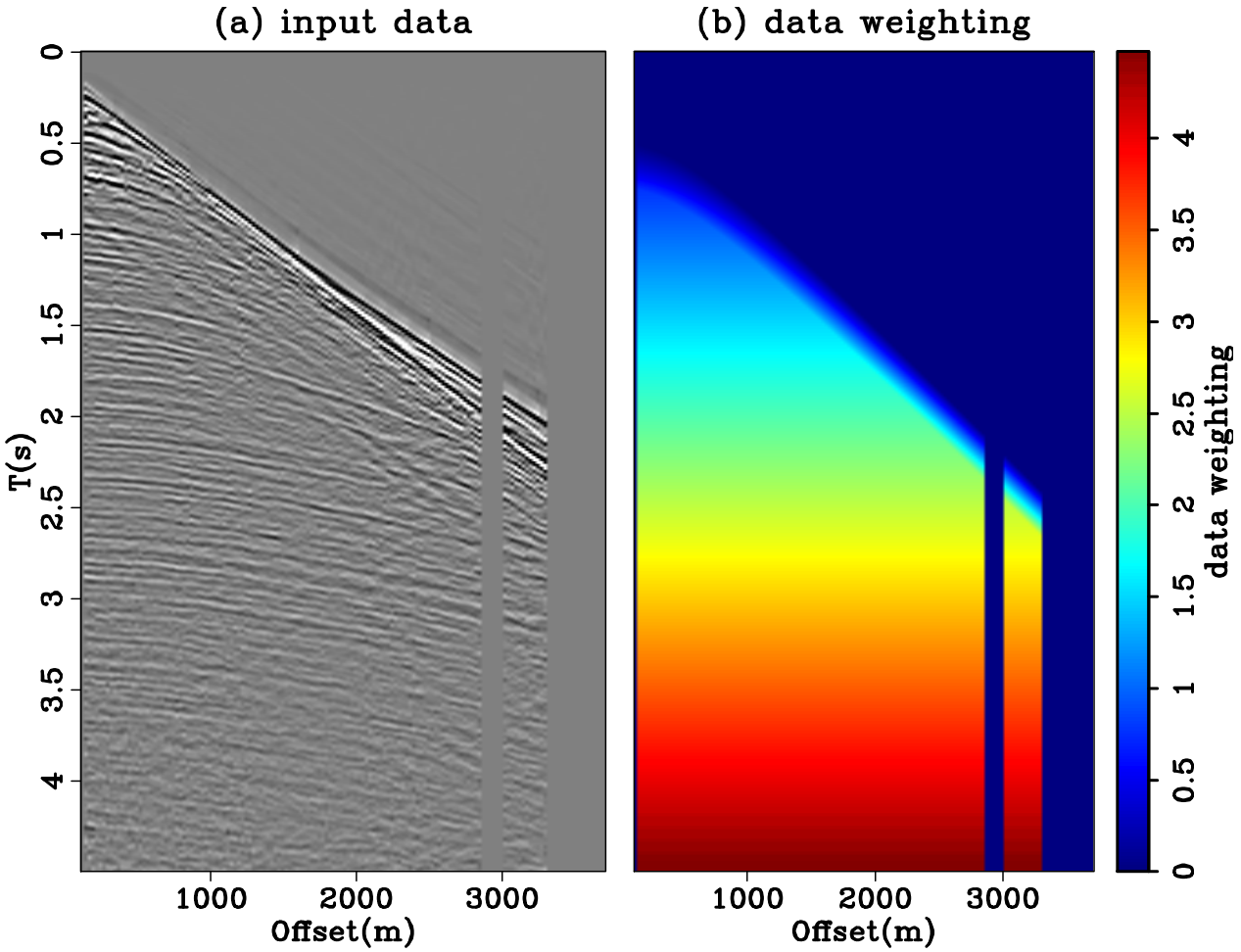

Figure 1: Input data for iterative migration in the sedimentary region. (a) is a shot gather. Notice the amplitude of the earlier reflection is much stronger than the deeper reflection. Therefore, (b) shows the data-weighting function used in the inversion to boost up the energy from the deeper part of the subsurface. The weighting function is also designed to exclude the direct arrival and head waves from the data-fitting part. [**ER**]

g_m, the images get more sparse due to the increased influence of the regularization term in the objective function (equation 3). Our selection of both parameters as our best result is based on two criteria: data fit comparable to the LSRTM result and sparseness content. The later can be quite subjective and left to the interpreter's opinion. A more systematic procedure would be preferable with larger 3-D datasets.

Sediment velocity model with salt

Now, we study a 2D line that cuts across a salt body. Figure 7a shows a shot gather. There are strong and fast refraction events that come from the top of salt layer. Similar to the sediment case, a diagonal data weighting (Figure 7b) is used in the iterative migration. Figure 8a shows the migration velocity model. The velocity value in the sediment layer increases gradually with depth. The salt body is shown in red with a velocity value close to 5000 m/s. Figure 8b shows the RTM image in this region. There are low-frequency artifacts above the salt body due to the application of the imaging condition to waves, in the receiver and shot wavefields, traveling in the same directions. The shallower reflectors are not well imaged due to the lack of illumination. In addition, there is a large amount of noise (coherent or spurious) within the salt body. These artifacts are better suppressed in the LSRTM image (Figure 9a) after 20 iterations. However, the shallow region remains noisy. With HPF iterative migration (Figure 9b), the above mentioned artifacts are better suppressed. The annotation highlight regions where the HPF image has fewer noise as compared to the LSRTM image. The HPF iterative migration image was generated using 20 iterations, a weighting value of $\epsilon = 0.005$ and a model-styling threshold of $g_m = 25$.

Figure 10a shows one shot gather from the input data. After 1 iteration, Figure 10b and 10c show the data residual from LSRTM and HPF iterative migration, respectively. Figure 10e and 10f show the corresponding data residual at iteration 20.

Figure 11 shows the normalized power spectrum in the z-direction between the RTM, the LSRTM, and the HPF iterative migration images. Notice that, with iterative inversion, the LSRTM and HPF spectrum becomes more white, especially in the higher and lower frequency range. There are higher frequency noise in the LSRTM, which are better suppressed with HPF iterative migration. We can see that the HPF image has an overall flatter spectrum as compared to the LSRTM image. The relative amplitude of the HPF image in the range of $kz = 0.004 - 0.012m^{-1}$ is higher than that from LSRTM.

DISCUSSION

Overall, we oberve that the HPF iterative migration can suppress migration artifacts in the image. However, the spareness constraint tends to make some reflectors less continuous. One way to improve on the current result is to add a geophysical

regularization term that enforces the continuity of amplitude along the reflectors. This require an estimation of the reflector's dip everywhere in the image and additional tuning parameters for the regularization term. A companion paper by Ma et al. (2014) has investigated the affects of including geophysical regularization in the iterative migration problem.

CONCLUSION

We compare inversion results of iterative migration using the classical least-squares norm and the hyperbolic penalty function. Reults from 2D field data examples show that using hyperbolic penalty function with model-styling can enforce sparsness in the image model. The sparse-reflectivity images obtained from hyperbolic penalty function iterative migration have less artifacts and better defined reflectors as compared to the LSRTM image. However, reflectors from the hyperbolic penalty function image are often less continuous and the parameterization of the hyperbolic penalty function remains cumbersome.

ACKNOWLEDGMENTS

Antoine Guitton acknowledges GeoImaging Solutions Inc. for financial support. The authors thank ExxonMobil for generously donatinng to SEP the field data used for the examples in this paper.

REFERENCES

Claerbout, J. F., 2014, Geophysical image estimation by examples.

Clapp, M. L., 2005, Imaging under salt: illumination compensation by regularized inversion: PhD thesis, Stanford University.

Li, Y., B. Biondi, R. Clapp, and D. Nichols, 2014, Wave-equation migration velocity analysis for VTI models: Geophysics, **79**, WA59–WA68.

Ma, Y., M. Maharramov, and B. Biondi, 2014, Geophysical application of hyperbolic and hybrid L1/L2 optimation: SEP Report, **155**.

Valenciano, A., 2008, Imaging by Wave-Equation Inversion: PhD thesis, Stanford University.

Wong, M., B. Biondi, and S. Ronen, 2012, Imaging with multiples using linearized full-wave inversion: SEG Expanded Abstracts, 1–5.

Wong, M. and A. Guitton, 2014, Preliminary results of iterative 1D imaging with the hybrid penalty function: SEP Report, **152**.

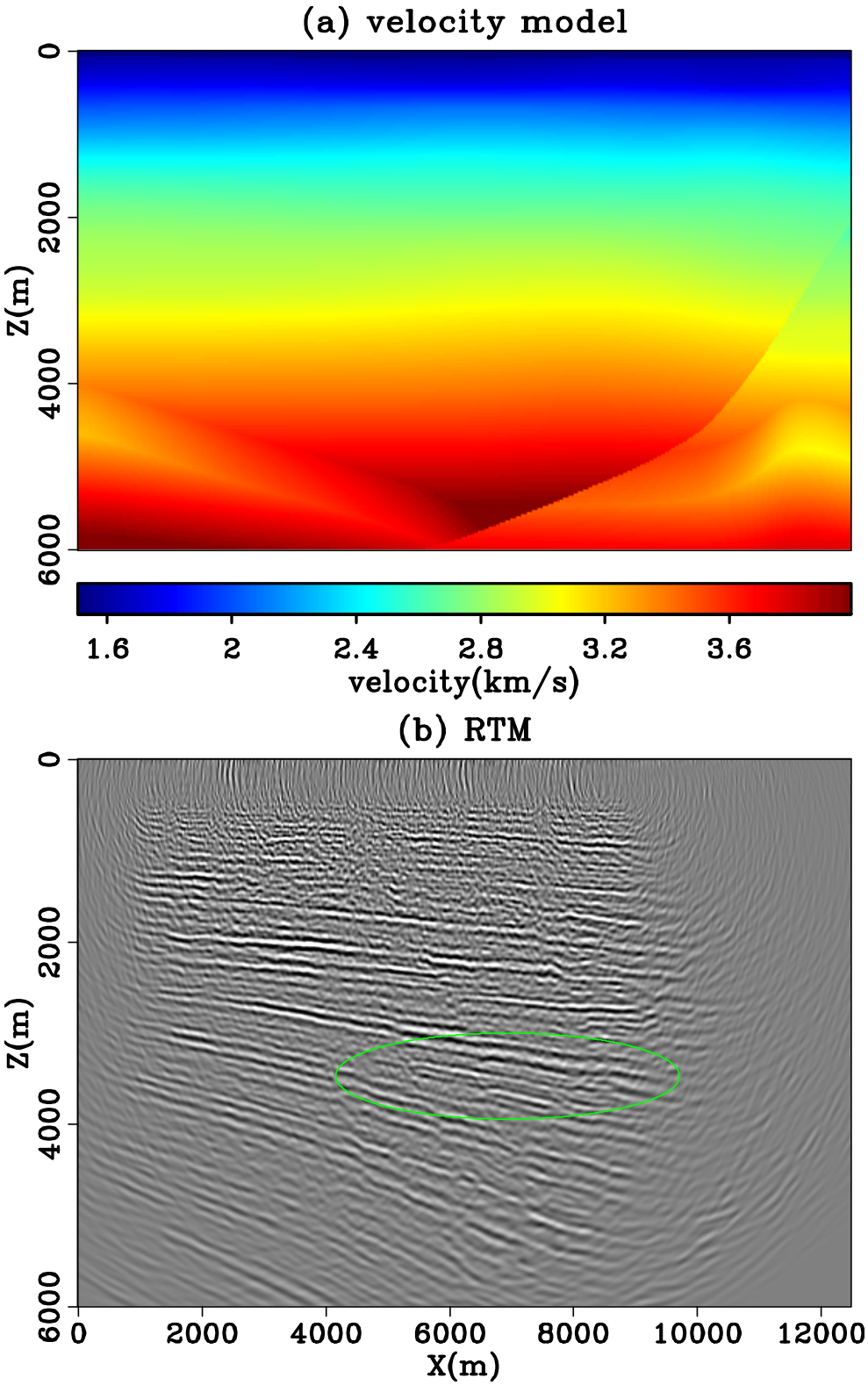

Figure 2: (a) The migration velocity model and (b) the RTM image. [**CR**]

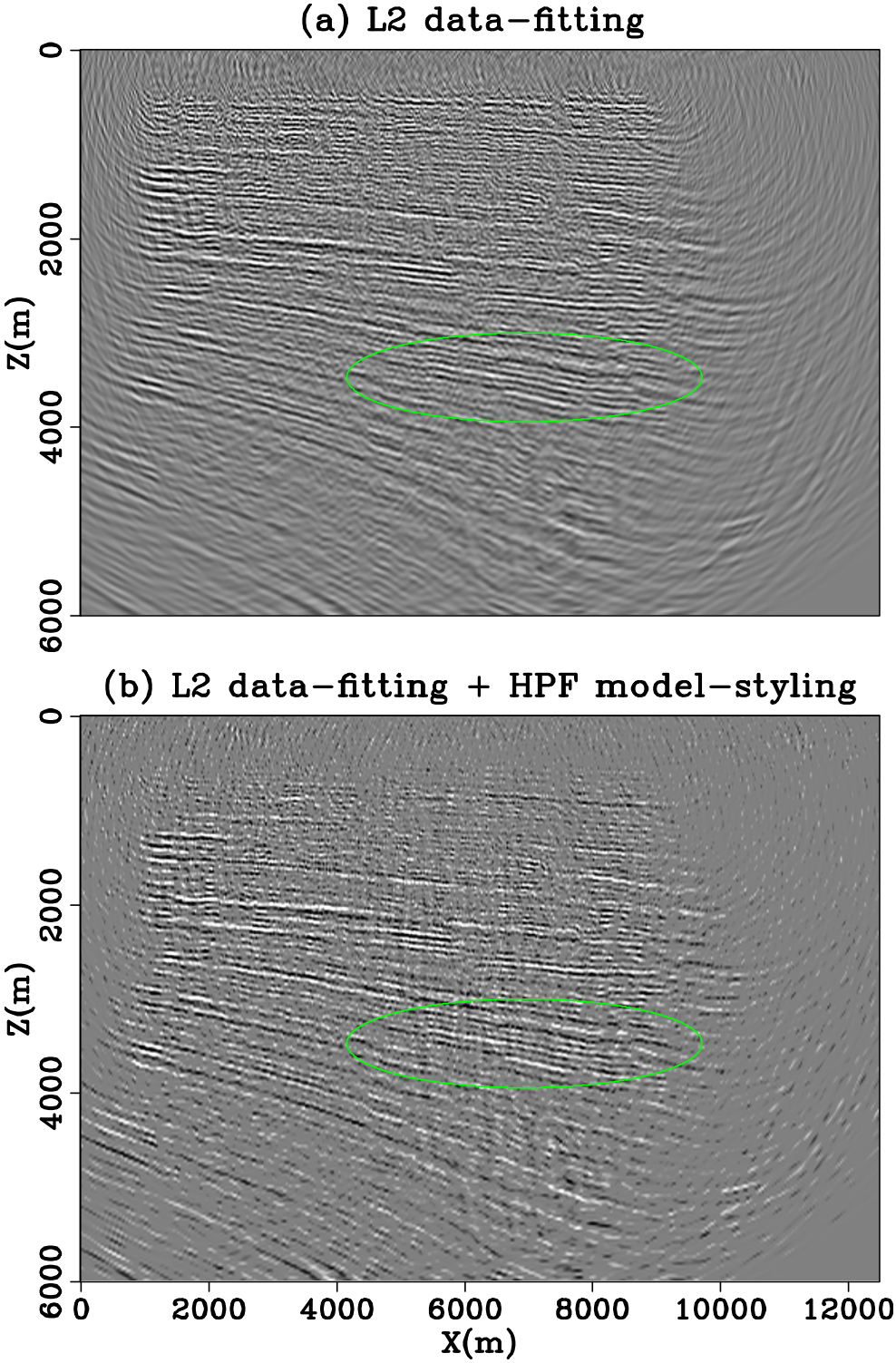

Figure 3: (a) LSRTM image using the ℓ^2 data-fitting objective function (equation 2) after 12 iterations of conjugate gradient algorithm. (b) The HPF iterative migration image using the ℓ^2 data-fitting with HPF model-styling objective function (3) after 20 iterations. [**CR**]

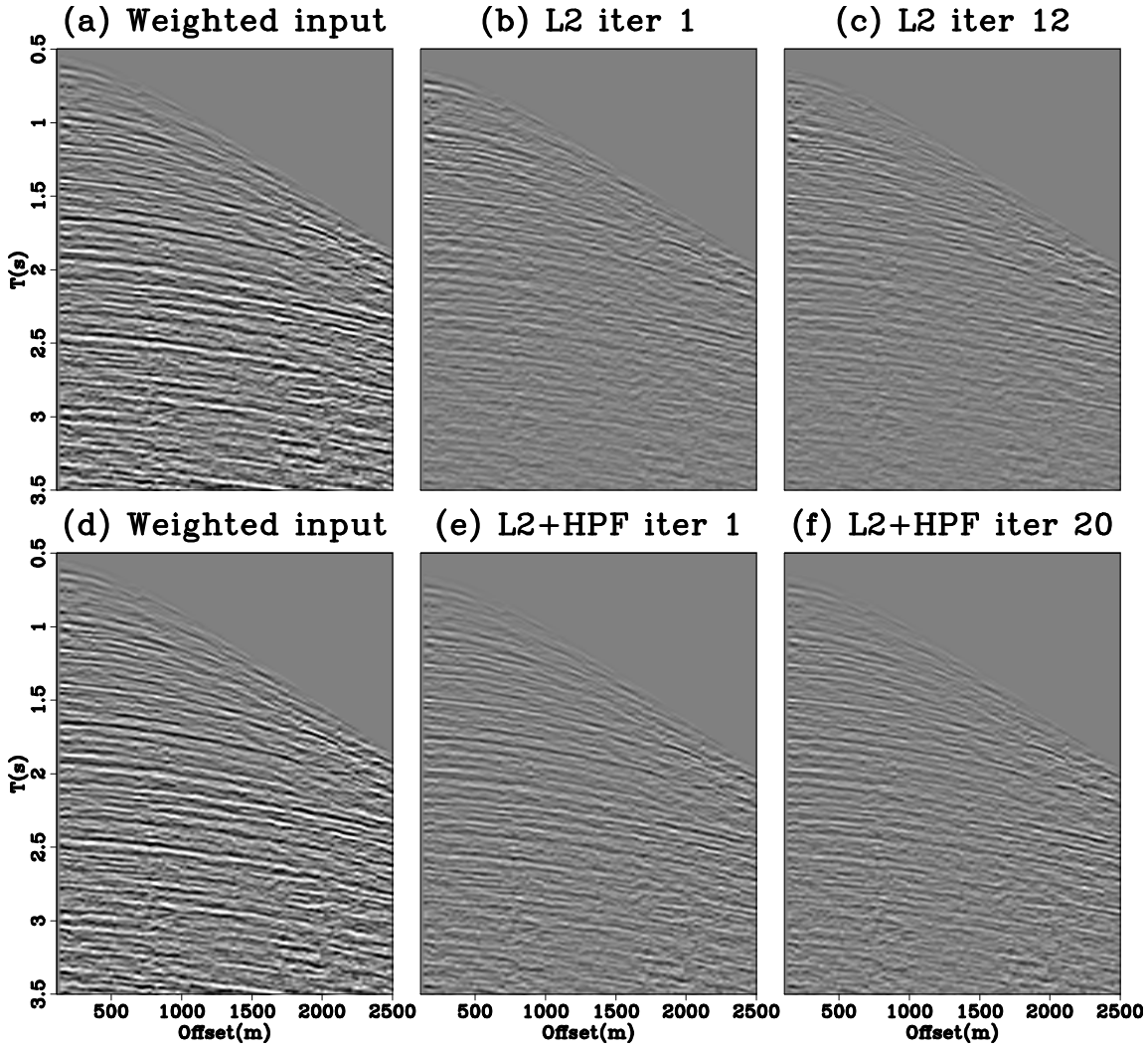

Figure 4: (a) and (d) shows one shot gather from the input data. The data residual from the same shot gather after (b) 1 iteration and (c) 12 iterations from LSRTM. The data residual from the same shot gather after (e) 1 iteration and (f) 20 iterations from the HPF iterative migration. All figures are clipped at the same level. [**CR**]

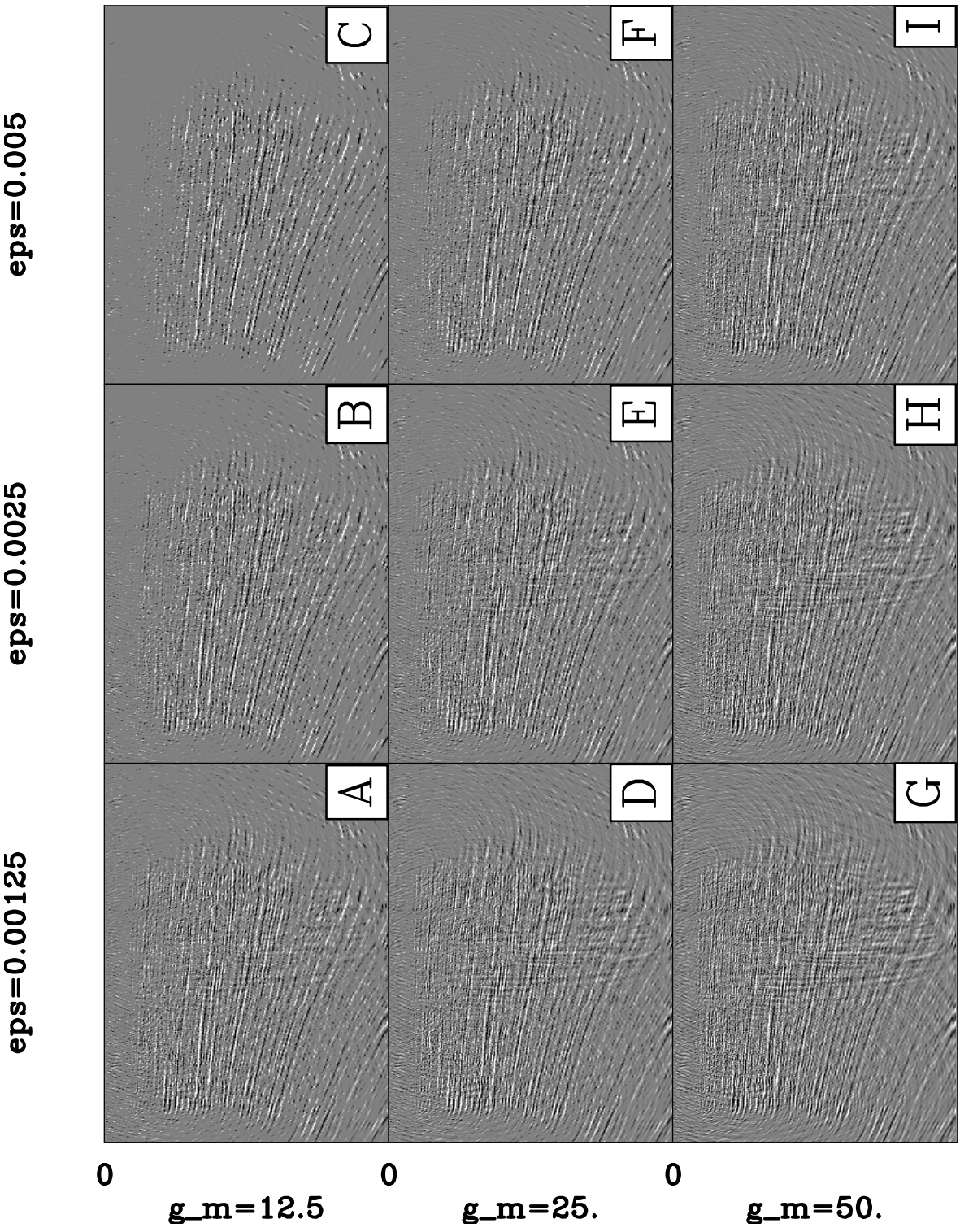

Figure 5: Inverted images from the HPF iterative migration using different ϵ and model-styling threshold values (g_m). Images from a common column use the same ϵ while images from a common row uses the same g_m. Panel A was selected as the HPF iterative migration result in Figure 3. [**CR**]

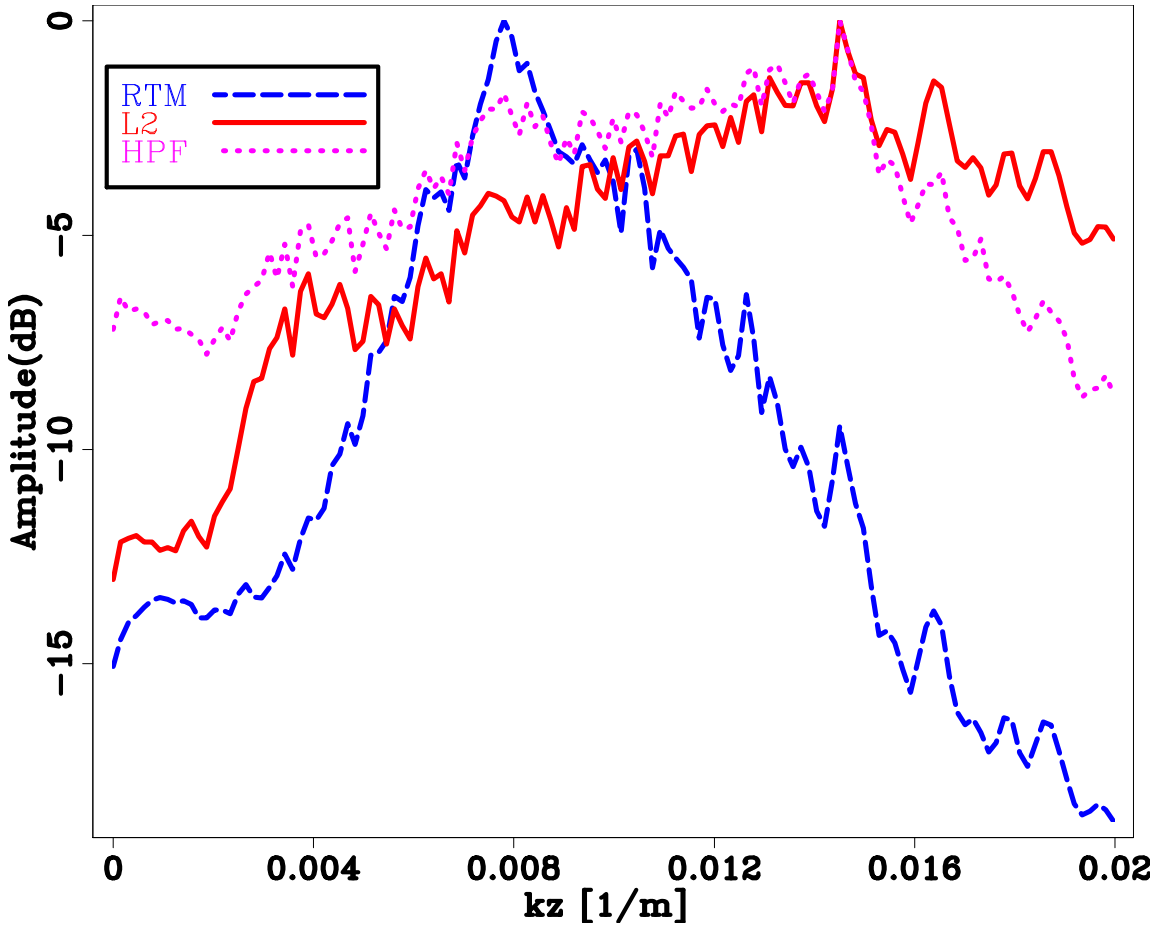

Figure 6: The normalized power spectrum in the z-direction for the RTM image, LSRTM image, and HPF iterative migration image from the first dataset. Iteration inversion raise the higher and lower end of the spectrum as compared to migration. [**CR**]

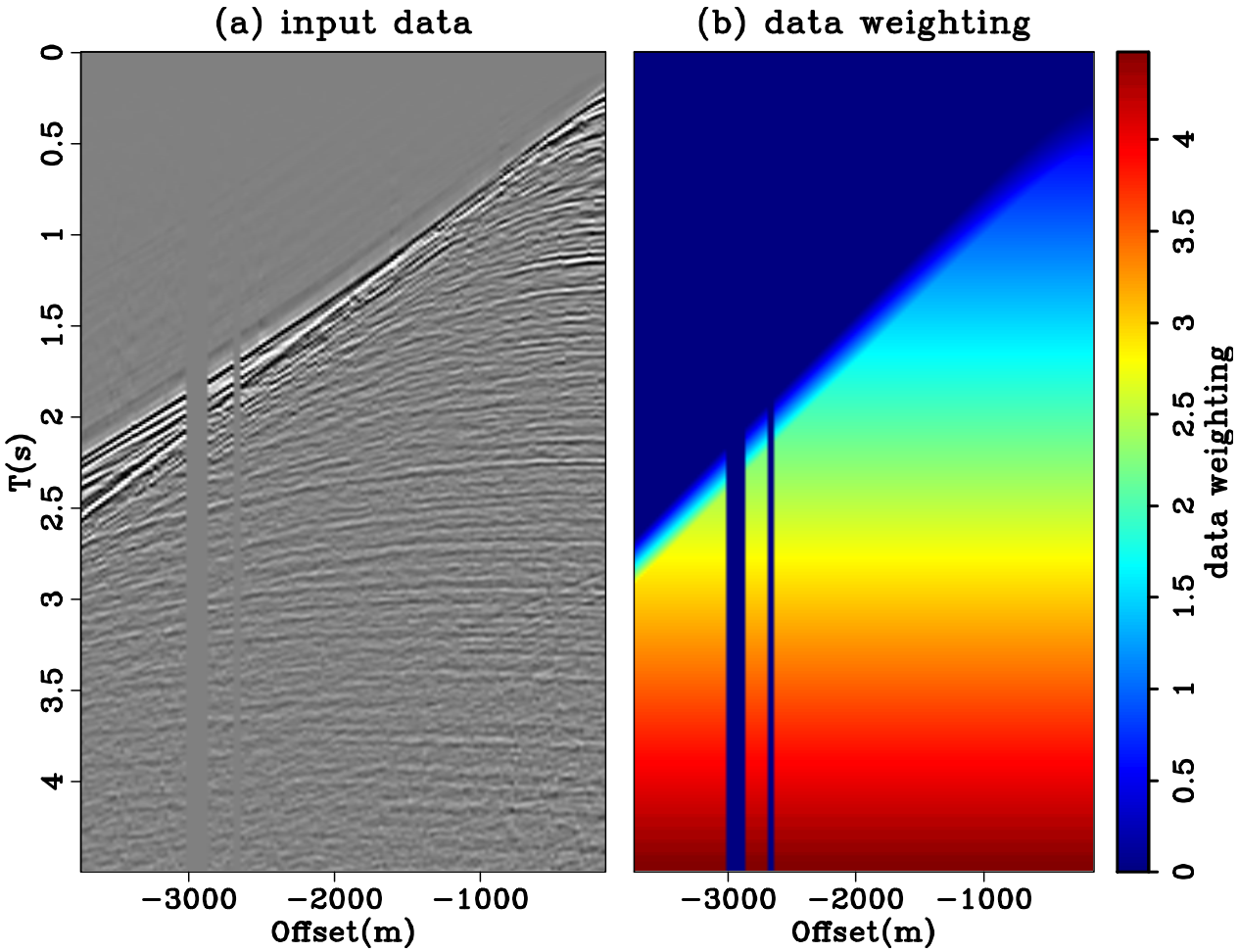

Figure 7: Input data for iterative migration in the salt region. (a) is a shot gather. The amplitude of the earlier reflection is much stronger than the deeper reflection. Therefore, (b) shows the data-weighting function used in the inversion to boost up the energy from the deeper part of the subsurface. [**ER**]

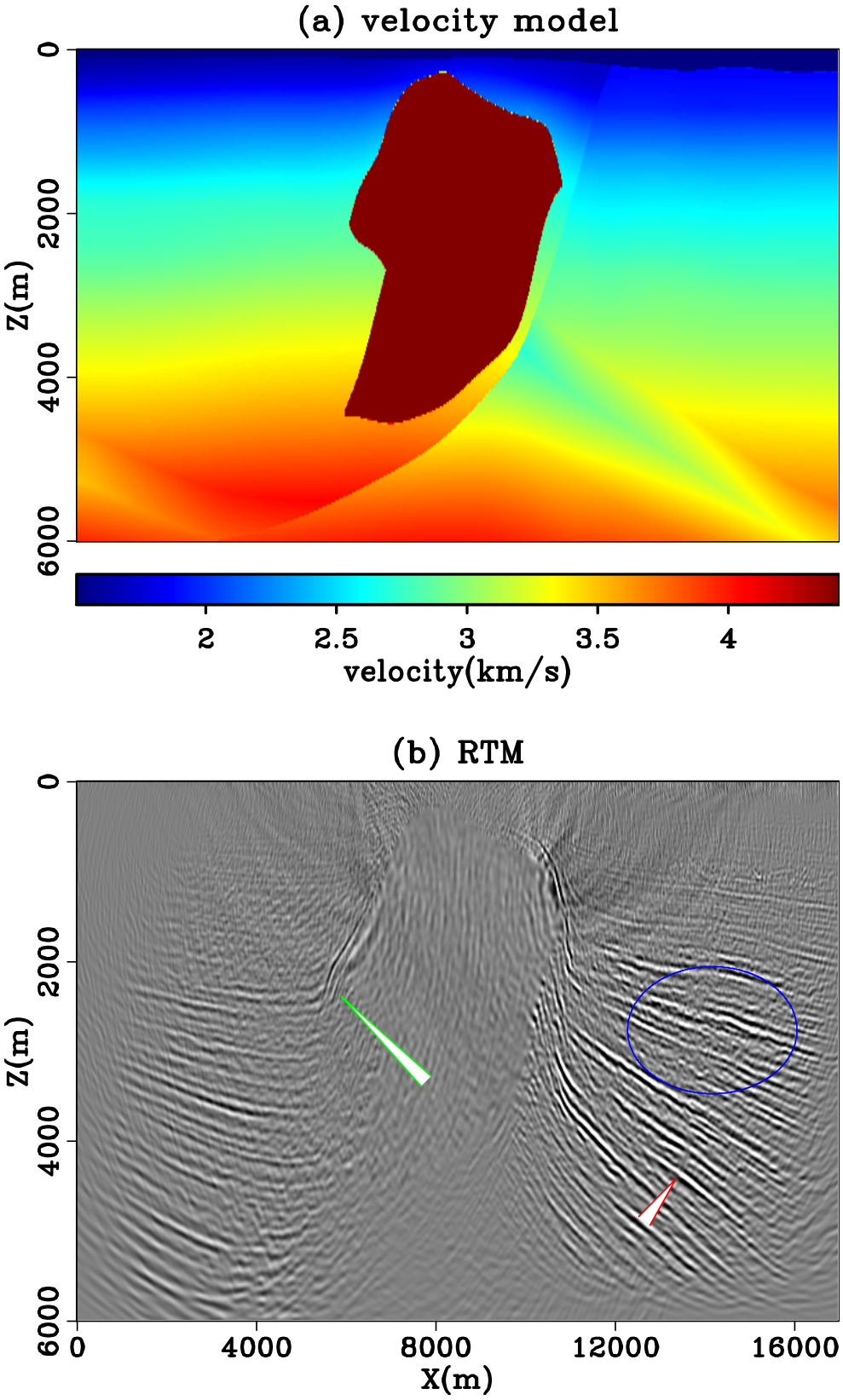

Figure 8: (a) The migration velocity model and (b) the RTM image. [**CR**]

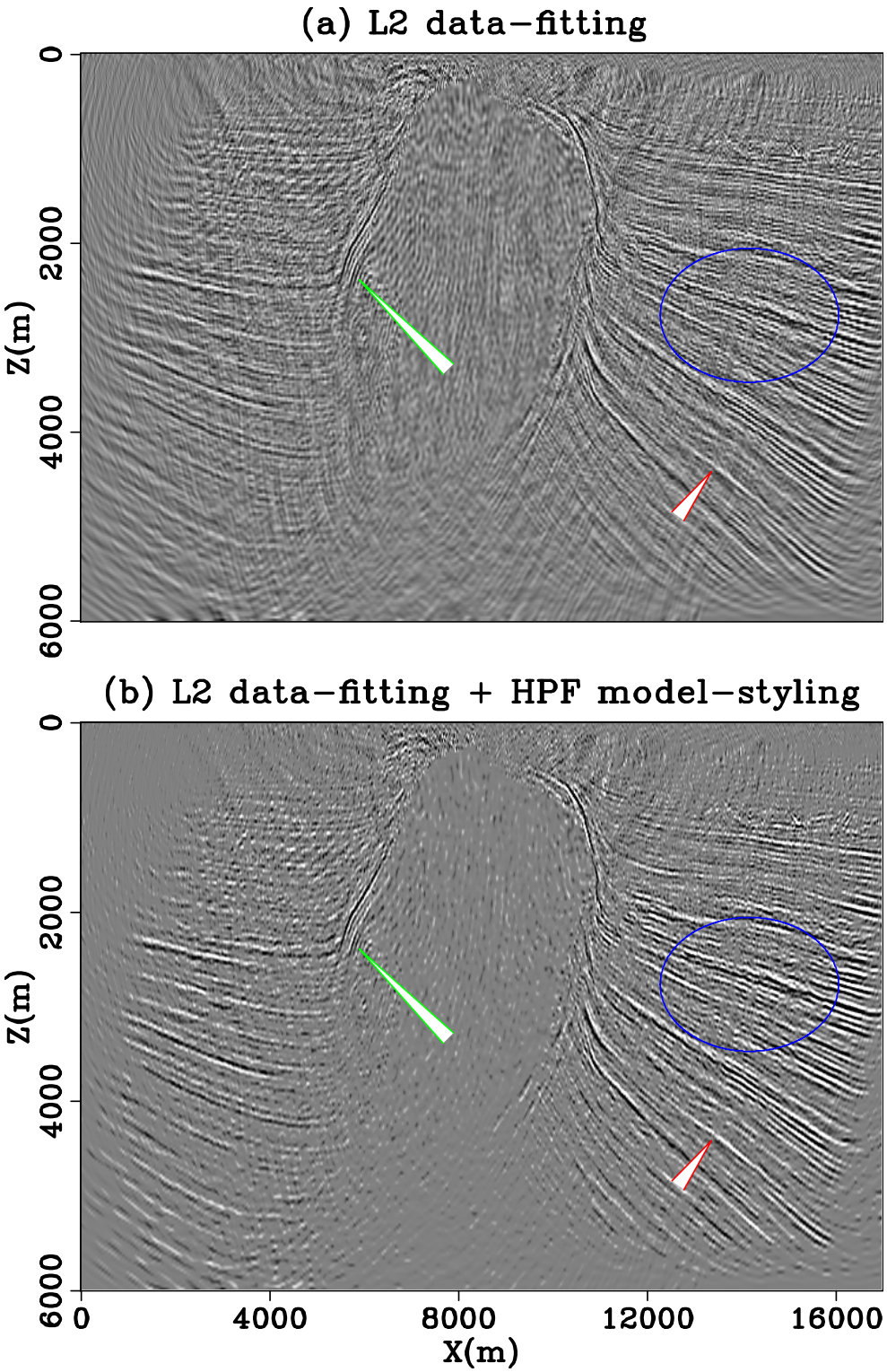

Figure 9: (a) The LSRTM image using the ℓ^2 data-fitting objective function (equation 2) and (b) the HPF iterative migration image using the ℓ^2 data-fitting with HPF model-styling objective function (3). Both inversions uses 20 iterations of the conjugate gradient algorithm. [**CR**]

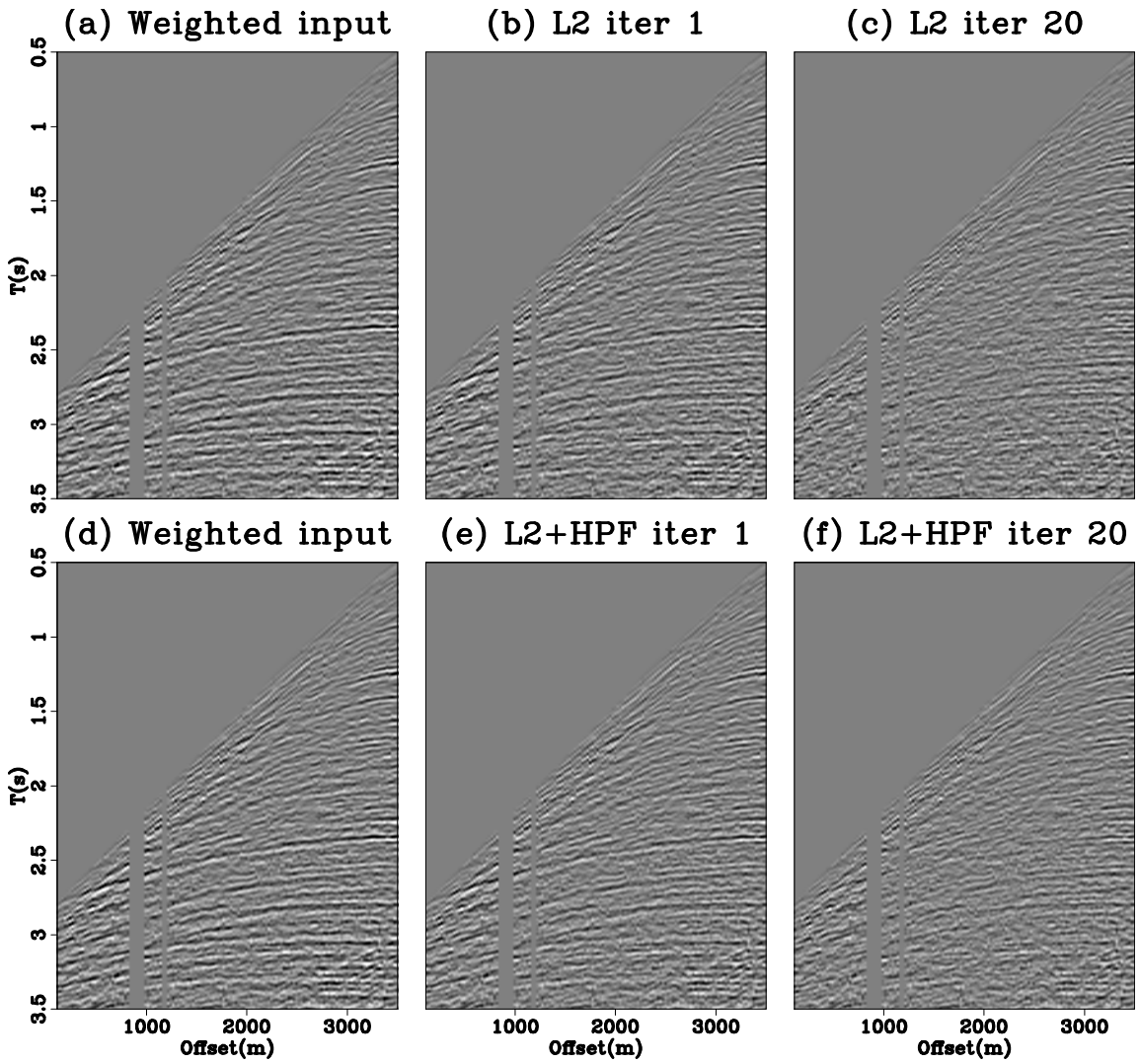

Figure 10: (a) and (d) shows one shot gather from the input data. The data residual from the same shot gather after (b) 1 iteration and (c) 20 iterations from LSRTM.The data residual from the same shot gather after (e) 1 iteration and (f) 20 iterations from the HPF iterative migration. All figures are clipped at the same level. [**CR**]

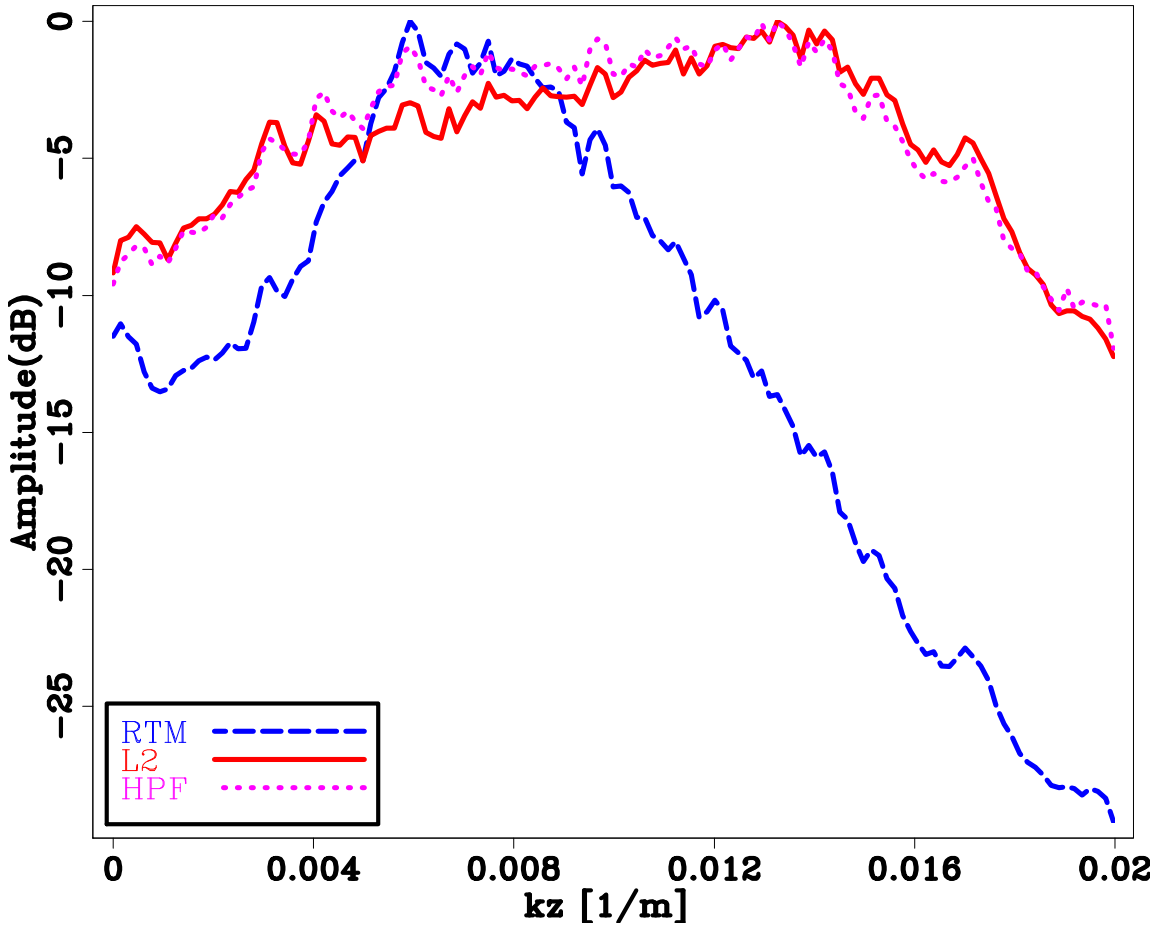

Figure 11: The normalized power spectrum in the z-direction for the RTM image, LSRTM image, and HPF iterative migration image from the second dataset. [**CR**]